Available online at www.sciencedirect.com

SciVerse ScienceDirect

Ceramics International 39 (2013) 1683–1694

CERAMICS INTERNATIONAL

www.elsevier.com/locate/ceramint

Synthesis, characterization and biological response of magnesium-substituted nanobioactive glass particles for biomedical applications

Muthusamy Prabhu[a], Kandiah Kavitha[a], Palanisamy Manivasakan[a], Venkatachalam Rajendran[a,*], Palanisami Kulandaivelu[b]

[a]*Centre for Nanoscience and Technology, K. S. Rangasamy College of Technology, Tiruchengode-637215, Namakkal (DT), Tamil Nadu, India*
[b]*Department of Mechanical Engineering, K. S. Rangasamy College of Technology,Tiruchengode-637215, Namakkal (DT), Tamil Nadu, India*

Received 22 June 2012; received in revised form 27 July 2012; accepted 4 August 2012
Available online 11 August 2012

Abstract

In this study, silica-based magnesium-substituted nanobioactive glass compositions ($58SiO_2$–$33CaO$–$9P_2O_5$, $58SiO_2$–$23CaO$–$9P_2O_5$–$10MgO$ and $58SiO_2$–$13CaO$–$9P_2O_5$–$20MgO$ (mol %)) were synthesized by a simple, cost-effective sol–gel method. The synthesized nanobioactive glass samples were characterized by X-ray diffraction, Fourier transform infrared spectroscopy, transmission electron microscopy, scanning electron microscopy and energy-dispersive X-ray fluorescence spectrometer studies. The prepared samples revealed amorphous phase with spherical morphology, having a particle size less than 50 nm. The samples MT0, MT10 and MT20 showed average pore diameters of 18.67, 17.35 and 24.51 nm while the specific surface areas were 90.69, 95.56 and 86.70 $m^2 g^{-1}$, respectively. The bioactivity of glass samples was confirmed by the formation of hydroxyapatite layer on glass surfaces during *in vitro* studies. Further, the MgO-doped nanobioactive glasses did not reveal significant antibacterial activity. A better biocompatibility was achieved in human gastric adenocarcinoma cell line in case of MgO glass samples while comparing the biological behaviour of MgO-based glasses with base glass. MgO substitutions show better *in vitro* bioactivity and remain non-cytotoxic to human cells.

Keywords: A. Sol–gel processes; B. Nanocomposites; D. MgO; E. Biomedical applications

1. Introduction

Over the last few decades, bioceramics have attracted attention because of their increasing application in treating damaged and infectious bones. Generally, bioceramics are broadly classified into bioinert (TiO_2, Al_2O_3 and ZrO_2), bioactive (hydroxyapatite (HAp)) and biodegradable (tri-calcium phosphate) ceramics. Nowadays, bioactive glasses are extensively used because of their unique properties such as rapid rate of surface reaction through chemical loading, low proportional softening temperature and easy designing of the required composition [1]. Bioactive glasses are mainly used in bone filling, implant coating and bone tissue engineering applications [2–5]. Generally, bioactive glasses are prepared using methods such as sol–gel [6], melt quenching [7] and sonication [8]. When compared with any of the existing preparation techniques, the sol–gel method has unique advantages such as low processing temperature, high purity, better homogeneity, microporosity and large surface area [9,10].

Bioactive glasses are the most promising biomaterials and show excellent bioactivity and biocompatibility when interacting with bone and tissue through the formation of HAp layer at the interface of the material [1,11]. The bioactivity of a bioactive glass is influenced by several factors such as composition, texture, density and porosity. Recent studies on different CaO–SiO_2 [12] and CaO–SiO_2–P_2O_5 [13–16] compositions of glass systems reveal good *in vitro* behaviour. Biologically active elements such as magnesium, sodium and phosphorus are generally substituted to glass systems to enhance their biocompatibility. Magnesium is one of the essential elements in the human body, and it is one of the main substitutes for Ca in biological apatites [17–19].

*Corresponding author. Tel.: +91 4288 274741 4x274880; fax: +91 4288 274880x274860.
E-mail address: veerajendran@gmail.com (V. Rajendran).

0272-8842/$ - see front matter © 2012 Elsevier Ltd and Techna Group S.r.l. All rights reserved.
http://dx.doi.org/10.1016/j.ceramint.2012.08.011

Diverse studies have been conducted to understand the role of bioactive glass constituents in determining the surface properties and *in vitro* formation of HAp layer. Although the role of SiO_2, CaO and P_2O_5 has been reviewed with reference to bioactivity, the effect of MgO on the glass ceramics and its *in vitro* bioactivity, the formation of apatite was delayed and decreased the degradability [20,21]. The role of MgO in the surface behaviour of bioglasses is contradictory, because it appears in the glass structure as a modifier or as a network former or as an intermediate. Hence, appropriate *in vitro* behaviour of MgO in silicate glasses is required even though it is found to inhibit mineralization in bones [22,23]. Few *in vitro* studies indicate that MgO inhibits mineralization [23] while others suggest that it does not affect apatite formation [24]. Recent investigations on the SiO_2–CaO–P_2O_5–MgO system show that high MgO content can promote *in vitro* apatite formation [25]. However, the information on the mechanism of apatite formation with different compositions of MgO and its influence on *in vitro* behaviour is scanty [26].

A review of the literature indicates the *in vitro* behaviour of MgO on base glass at micro scale. Besides, the incorporation of MgO in nano-bioactive glass may be better than in the bulk glasses because of high surface to volume ratio and higher reactivity. Therefore, the synthesis and characterization of MgO-substituted nano-SiO_2–CaO–P_2O_5 base glasses are increasing because of its high mechanical properties, bioactivity and biocompatibility.

The objectives of this investigation were to synthesize and characterize the different compositions ($x=0$, 10 and 20 mol%) of MgO-substituted nanobioactive glass powders ($58SiO_2$–(33-x) CaO–xMgO–$9P_2O_5$) for better understanding of the changes in physicochemical properties of bioglasses. The antimicrobial property of the synthesized glass powders was explored using clinical pathogens such as *Staphylococcus aureus* and *Escherichia coli* for different biomedical applications. The effect of MgO-substituted nanobioactive glasses on *in vitro* bioactivity was also examined using simulated body fluid (SBF) and human gastric adenocarcinoma (AGS) cell line.

2. Materials and methods

2.1. Preparation of reagents and standard solutions

Silica-based nanobioactive glasses of 58% SiO_2–(33-x) CaO–9% P_2O_5–x% MgO for different compositions of $x=0$, 10 and 20 mol% were prepared (hereafter termed as MT0, MT10 and MT20) through the sol–gel method [11,27]. The compositions of the prepared glass powders in mol% are given in Table 1. The chemical precursors used in this study were tetraethyl orthosilicate ($Si(OC_2H_5)_4$; Sigma-Aldrich, min. 99%), triethyl phosphate ($(CH_3CH_2O)_3P(O)$; HiMedia, Mumbai, India, min. 99.5%), calcium nitrate ($Ca(NO_3)_2\cdot 4H_2O$; Merck, min. 98% GR), magnesium nitrate ($MgNO_3$; Merck, min. 99% GR), 2 N nitric acid (HNO_3; Merck, min. 69% GR), ethanol, 1 M ammonia (Merck, min. 25% GR) and ultrapure water (Arium 611UF; Sartorius AG). All the reagents were used as received without any further purification.

Table 1
Compositions of prepared nanobioactive glass samples.

Sample code	Compositions (mol%)			
	SiO_2	CaO	P_2O_5	MgO
MT0	58	33	9	0
MT10	58	23	9	10
MT20	58	13	9	20

2.2. Synthesis of nanobioactive glass powders

Initially, tetraethyl orthosilicate (TEOS) was dissolved in 1:1 ratio of ethanol and distilled water. Then, 2 N nitric acid was added to the solution while stirring at room temperature for 30 min. After the complete hydrolysis of TEOS, triethyl phosphate, calcium nitrate and magnesium nitrate were consequently added to the obtained solution at 30 min intervals under constant stirring. Ammonia solution (1 M) was added to the solution until the formation of a gel, that is, until the solution reaches its pH ~ 8.0. Thereafter, the resulting gel was aged for 2 day in a hot air oven at 60 °C and then, it was dried at 120 °C for 2 day. The obtained powder was ground with a dry ball milling technique using zirconium balls at a speed of 400 rpm for 1 h. The grounded samples were calcinated at 600 °C for 4 h to remove the carbon and nitrate impurities.

2.3. Characterization

2.3.1. X-ray diffraction

The structural nature of nanobioactive glass powders and the formation of HAp layer on glass surface during *in vitro* studies were characterized through X-ray diffraction (XRD) analysis using an X-ray diffractometer (X' PertPro, PANalytical, Almelo, the Netherlands) with Cu K_α as the radiation ($\lambda=1.5418$ Å) source. The source was operated at 40 kV with 2θ value varying from 10° to 80°.

2.3.2. Surface area analysis

The specific surface area (SSA) of prepared nanobioactive glass particles was measured by the Barrett–Emmett–Teller (BET) method [28] using the BET surface area (Autosorp AS-1MP; Quantachrome, Boynton Beach, FL, USA) pore size analyser. The sample was degassed for 3 h at 295 °C and the physisorption analysis was performed with N_2 adsorption measurements at liquid N_2 temperature (−196 °C). The very low temperature was used to avoid any thermally induced changes on the surface of the particle. Three-point BET correlation techniques were used

to determine the SSA of the prepared nanobioactive glass particles.

2.3.3. Fourier transform infrared spectroscopy

The infrared absorption spectra of nanobioactive glass powder samples were analyzed at room temperature in the wave number range of 4000–400 cm^{-1} using Fourier transform infrared (FTIR) spectrometer (Spectrum 100; PerkinElmer, USA). The prepared samples each of 2 mg were mixed with 200 mg KBr in an agate mortar and pressed into a pellet. For each sample, the FTIR spectrum was normalized with a blank KBr pellet. These measurements were done for the prepared glass compositions before and after *in vitro* studies.

2.3.4. X-ray fluorescence spectrometry

Elemental compositions of the prepared nanobioactive glass samples were ascertained using X-ray fluorescence (XRF) spectrometer (EDX-720; Shimadzu, Kyoto, Japan) to explore the weight loss of the prepared materials during synthesis and after *in vitro* studies.

2.3.5. Electron microscopy

Particle size and morphology of the prepared nanobioactive glass powders were determined using images obtained from transmission electron microscopy (TEM) (CM 200; Philips, USA). The surface morphology and elements present in the prepared samples were analyzed using scanning electron microscope coupled with an energy-dispersive X-ray analysis (JSM 6360; JEOL, Japan).

2.3.6. In vitro bioactivity

Bioactivity of the prepared nanobioactive glass powders was ascertained through *in vitro* studies using SBF solution to explore the formation of HAp layer on the surface of the prepared sample. The SBF solution was prepared using the standard protocol [29] where the pH value was 7.4 that is equivalent to the pH value of human blood plasma. A volume of 250 mg of the prepared nanobioactive glass powders was transferred separately into a polyurethane bottle containing 50 ml SBF solution and incubated at 37 °C for 21 day. The ionic changes in the SBF solution were monitored by measuring the changes in pH value for every day over a period of 21 day using a pH electrode (Thermo Orion 720A; 3 Star, USA). The electrode was calibrated using the standard pH values of 4.0, 7.0 and 10.01 before starting the pH measurements. The samples were removed from SBF solution after 21 day of *in vitro* studies and gently washed with distilled water and allowed to dry. The dried samples were used for further characterization studies such as XRD, FTIR, SEM and XRF analysis to reveal the formation of HAp layer on the surface of glass samples. The weight loss% of each sample was calculated using the following Eq. (1):

$$\text{Weight loss}\% = [W_0 - W_t / W_0] \times 100 \quad (1)$$

where W_0 is the initial weight of the each sample and W_t the weight of the each sample measured at time t after being dried.

2.3.7. Antibacterial activity

Antimicrobial property of the bioactive glass samples was tested against clinical pathogens such as *S. aureus* and *E. coli* using the Kirby–Bauer disc diffusion method [30]. Mueller hinton agar (MHA) medium (Hi Media) was prepared and sterilized at 121 °C (15 psi). The MHA plates were prepared by pouring 15 ml molten medium into sterile petri plates. The plates were allowed to solidify for about 5 min and 0.1% of inoculum suspension was swabbed uniformly over the agar until the inoculum became invisible. Different concentrations (0, 10, 100 and 1000 $\mu g\, l^{-1}$) of nanobioactive glass powders were loaded onto 5 mm sterile individual discs, followed by incubation of plates at 37 °C for 24 h. Antibiotics like Streptomycin and Amoxicillin (10 $\mu g\, L^{-1}$) were used as positive control for gram positive and gram negative bacteria. After incubation, the plates were observed for the zone of inhibition around the disc and measured with a transparent millimeter ruler. The above study was performed in triplicate.

2.3.8. Cell culture and cytotoxicity assay

Human gastric adenocarcinoma (AGS) cell line (ATCC-1739) was obtained from the National Centre for Cell Science, Pune, India. The cells were grown and maintained in Dulbecco's modified Eagle's medium (DMEM)/nutrient mixture F-12 HAM (1:1) with 2 $mM\, L^{-1}$ glutamine supplemented with 10% fetal bovine serum, 45 IU ml^{-1} penicillin and 45 IU ml^{-1} streptomycin. Growth ingredients were also added and incubated in a humidified atmosphere at 37 °C in 5% CO_2. After a number of passaging, the pure confluent AGS cell lines were obtained and cells at a density of 10^3 were used to evaluate the cytotoxicity at a concentration of 100 $\mu g\, ml^{-1}$ for all the prepared nanobioactive glass samples. The morphology of AGS cell lines was observed regularly under binocular inverted microscope. After 48 h of incubation, MTT (3-(4,5-dimethylthiazol-2-yl)-2,5-diphenyltetrazolium bromide) assay was performed to evaluate the viability of the nanobioactive glass-treated AGS cells. The percentage of cell viability from triplicates of the nanobioactive glass-treated and non-treated cells was calculated using optical density (OD 590 nm) as follows:

$$\text{Cell viability}\% = \frac{\text{OD of the nanoparticles treated cells}}{\text{OD of the cells}} \times 100$$

3. Results and discussion

The XRD patterns of the prepared nanobioactive glass samples with different concentrations of magnesium ions are shown in Fig. 1. These patterns show an amorphous

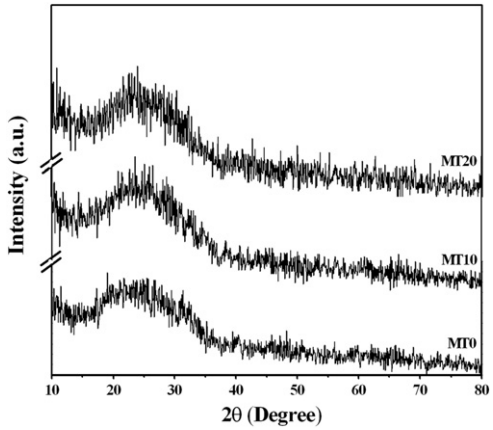

Fig. 1. XRD pattern of prepared nanobioactive glass powders.

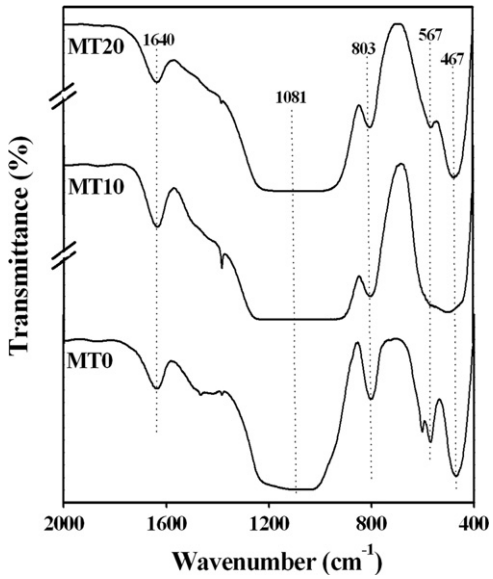

Fig. 2. FTIR spectra of prepared nanobioactive glass powders.

nature, revealing that the composition of MgO in the base glass system does not influence the crystallization of bioactive glasses. The FTIR spectra of the prepared nanobioactive glass samples (MT0, MT10 and MT20) are given in Fig. 2. The bands observed along with the assigned peaks are listed in Table 2. Silicate network absorption bands are observed at 1081, 803 and 467 cm^{-1} which are assigned to the asymmetric stretching mode, symmetric stretching mode and the stretching vibration of Si–O–Si, respectively. The above peaks confirm the presence of silica in the glass systems [31]. Table 3 summarizes the textural analysis of prepared nanobioactive glass samples. The average pore diameters of MT0, MT10 and MT20 nanobioactive glass samples lie in the range of 18.67, 17.35 and 24.51 nm, respectively. It can be seen from the pore size analysis that all the nano bioactive glass samples are in the mesoporous range. The SSA of MT0, MT10 and MT20 glass samples are 90.69, 95.56 and

Table 2
Frequencies and assignments of IR absorption bands in the spectra of before and after *in vitro* studies of prepared samples.

Observed bands (cm^{-1})	Peak assignments
1643, 1640	O–H bending (molecular water) [48]
1455, 1418	C–O stretching vibration band [49]
1090, 1081	Asymmetric Si–O–Si stretching in SiO_4 tetrahedron [48]
874	C–O stretching vibration band [49,50]
802, 803	Symmetric Si–O–Si stretching in SiO_4 tetrahedron [48]
603	–P=O bending band [51], phosphate PO_4^{-3} vibration band [48]
567, 564	phosphate PO_3^{-2} vibration band [48]
469, 467	Si–O–Si stretching [48]

Table 3
Textural properties of nanobioactive glass particles.

Sample code	Surface area ($m^2\ g^{-1}$)	Average pore diameter (nm)	Total pore volume ($cm^3\ g^{-1}$)
MT0	90.69	18.67	0.415
MT10	95.56	17.35	0.65
MT20	86.70	24.51	0.531

86.70 $m^2\ g^{-1}$, respectively. It can be concluded that the high surface area of sol–gel derived nano bioactive glass samples facilitates the efficient formation of HAp layer on the glass surface when compared with melt-derived glasses [12,32].

Size and morphology of the prepared nanobioactive glass were confirmed through TEM analysis (Fig. 3). MT10 glass sample shows a uniform spherical shape with a well-dispersed particle size of below 50 nm (Fig. 3b). The images of MT0 and MT20 glass samples are observed to be closely agglomerated particles with non-uniform shapes as shown in Fig. 3a and c. However, the diffraction pattern (inset in Fig. 3) confirms the amorphous nature of the prepared nano-bioactive glasses [8]. The observed morphological changes in MgO-based glass systems are due to interchange of Mg with Ca that stimulates structural modifications [33–35] and acts as an intermediate when the concentration of Mg increases to 20% [36]. It has been projected that the substitution of more than 10% MgO on nanobioactive glasses may decrease the bioactivity of silica-based glasses.

SEM images and the corresponding EDX spectrum of the prepared nanobioactive glass samples are shown in Fig. 4. MT0 (Fig. 4a) glass powders exhibit an agglomerated and rough spherical surface with irregular morphology compared with MgO-substituted glasses. The surface of MgO-substituted glass samples MT10 and MT20 became denser with increasing MgO concentration in silica glasses shown in Fig. 4b and c, respectively. A good spherical morphology with uniform particle size is observed in the MT10 glass samples. On the other hand,

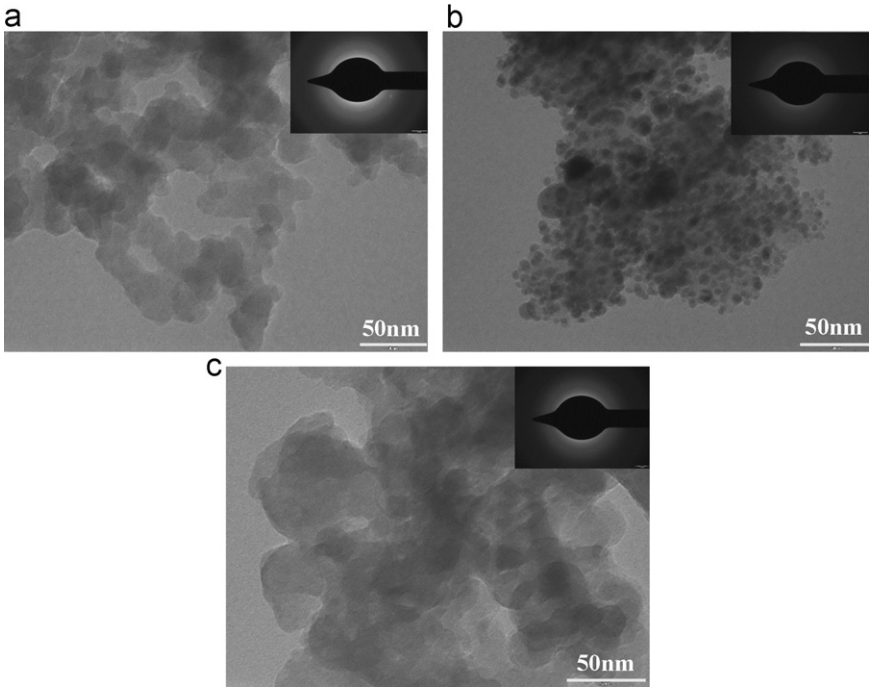

Fig. 3. TEM images and corresponding diffraction pattern of different nano bioactive glass samples. (a) MT0, (b) MT10 and (c) MT20.

the EDX pattern of all the samples has 98% purity with negligible carbon content. It can be concluded from the above results that an increase in the concentration of magnesium above 10% leads to an irregular morphology with aggregated particles.

The changes in pH of the SBF solution after immersion of samples for a period of 21 day are shown in Fig. 5. The above results help to explore the changes in the *in vitro* behaviour of glass systems with respect to MgO addition. The pH variations at different days indicate that the ion exchange takes place between the samples and SBF solution. Fig. 5 shows a marked increase in pH value of all samples up to third day. This may be because of the release of ions from the sample in SBF solution. When compared with base (MT0) glass, MgO-substituted glass samples reveal a high pH on the first day because of the presence of magnesium ions in powder. At 15th day, the solution shows a decrease in pH value of all the samples due to the deposition or precipitation of calcium phosphates and carbonates on bioactive glass powders. However, after the 15th day, there is no significant variation in any sample. On the other hand, MT10 maintains the stationary phase from 15 to 21 day, which may be due to the saturation of ion exchange after the formation of HAp layer in SBF solution. Further, harvested powders from SBF solution are characterized by XRD, FTIR and XRF studies.

The weight loss of nanobioactive glass samples after 21 day of incubation in SBF solution is shown in Fig. 6. The degradation rate of MT0, MT10 and MT20 glass samples are 16.26%, 19.85% and 17.35%, respectively. The Mg-substituted nanobioactive glass sample (MT10) shows an increased weight loss when compared with MT0 and MT20 samples. This indicates that MgO plays a crucial role in the weight loss and the partial substitution for CaO which interns to increase the glass degradability. As the substitution of MgO increases up to 10%, it leads to increase in the formation of apatite layer on the glass surface. On the other hand, when the concentration of Mg increases beyond 10 (mol%), the degradation rate decreases, as a result delaying the formation of apatite layer on the glass surface. The weight loss result shows that the apatite layer formation ability is related to its solubility. A decreased value of solubility reveals a lower bioactivity which is in line with the earlier studies [37].

The XRD pattern of the glass powders after 21 day of immersion in SBF is shown in Fig. 7. The diffraction peaks observed at 25.8°, 31.9°, 35.4°, 49.69° and 53.35° (JCPDS no.: 09-0432) correspond to the crystalline peaks of HAp layer that is formed on the surface of the nanobioactive glass powders [38]. The observed results clearly indicate the strong formation of HAp in MT10 samples compared with MT0 and MT20 samples. However, the rate of HAp formation on MT10 bioactive glass is higher than that on other bioactive glass samples, which confirms that 10% MgO-substituted bioactive glass has a better bioactivity. Mg acts as one of the main substitutes for Ca in biological apatite formation, which is in accordance with our results [17]. When the concentration of Mg increases more than 10%, it acts as an intermediate that suppresses dissolution rate and also reduces the rate of formation of HAp layer. From the above results, it is justified that minimum 23% of calcium is essential in Mg-substituted bioactive glass to maintain the bioactivity for the formation of HAp layer.

The FTIR spectra of all the samples after soaking in SBF for 21 day are presented in Fig. 8. The absorption of the

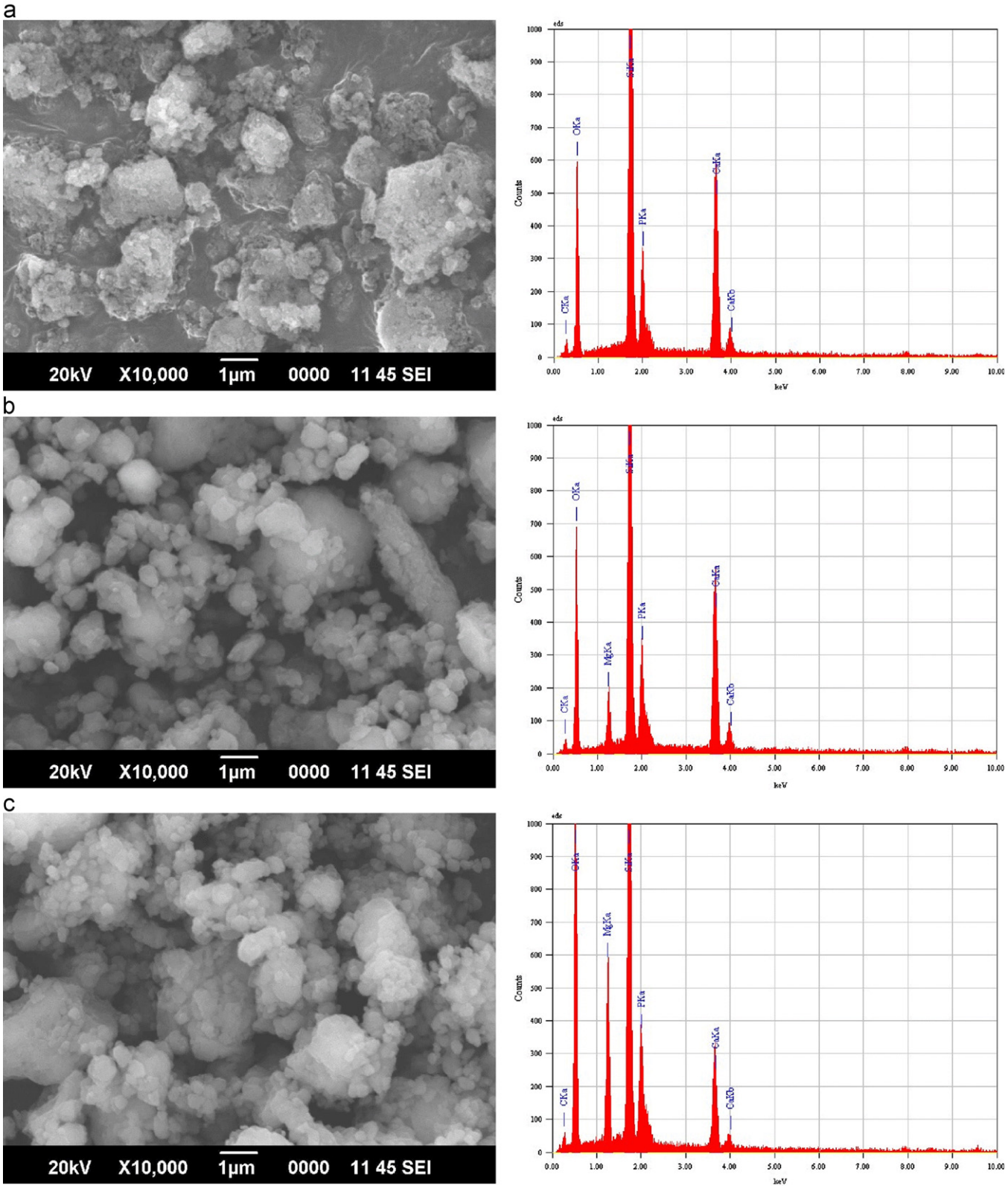

Fig. 4. SEM images with corresponding EDX pattern of different nanobioactive glass samples. (a) MT0, (b) MT10 and (c) MT20.

phosphate band observed at 603 and 564 cm^{-1} confirms the formation of a calcium phosphate layer in the crystalline phase [39,40]. In addition, carbonate absorption peaks at 1455, 1418 and 874 cm^{-1} are also detected in the MT10 sample. However, it is concluded that the evolution of carbonate band is higher in MT10 samples than in other samples after 21 day. The well-observed carbonate and phosphate bands indicate the formation of an apatite layer

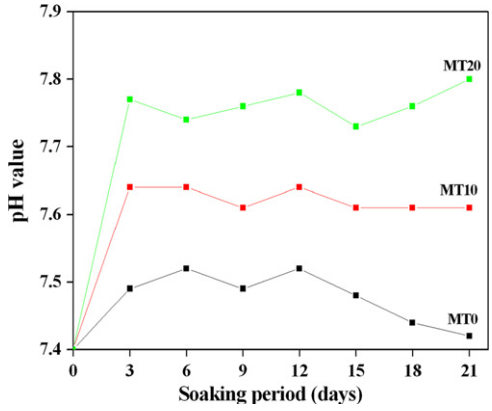

Fig. 5. pH variation in different soaking periods for the glass samples.

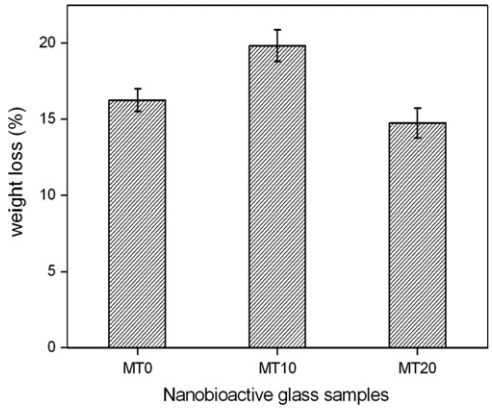

Fig. 6. Weight loss % of prepared samples after 21 day of immersion in SBF solution.

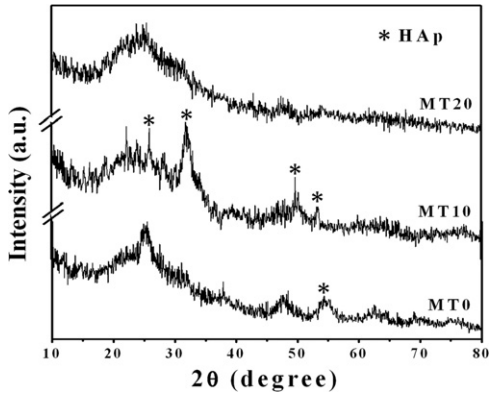

Fig. 7. XRD pattern of nanobioactive glass powders after 21 day of incubation in SBF solution.

on the surface of bioactive glass samples. In addition, it also confirms that the well-formed material is carbonate HAp in present glasses [41]. In particular, the increased bioactivity of 10% Mg-substituted nanobioactive glass may be because of fast dissolution of Ca^{2+} and P^{5+} ions on the surface.

The SEM micrographs of all the glass samples (MT0, MT10 and MT20) after soaking in SBF for 21 day are shown in Fig. 9a–c, respectively. An obvious difference in the surface morphology of the glass samples is observed before and after

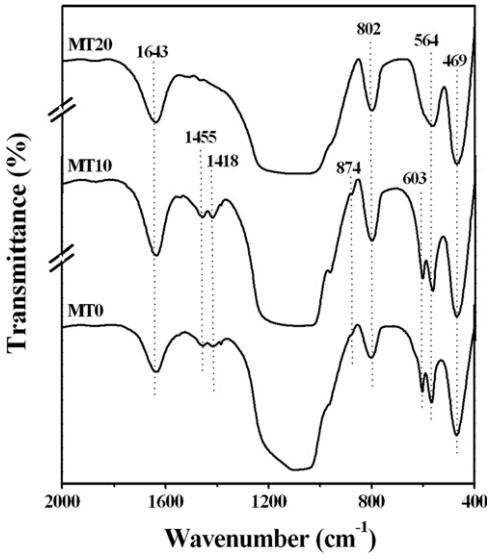

Fig. 8. FTIR spectra of nanobioactive glass powder after incubation in SBF solution for 21 day.

immersion in SBF, indicating the formation of a new apatite layer on the surface. The glass without MgO content (MT0) shows a lesser formation of HAp layer on its surface after *in vitro* studies. A thick layer of HAp is noticed on the surface of MT10 glass samples (Fig. 9b) when compared to other MgO-substituted glass samples. The above results conclude that the reactivity of MT10 is high with SBF and hence, the glass surface is fully covered with a crystalline HAp layer without any interface. This may be due to the interchange of magnesium ions by calcium ions. As the concentration of Mg increases above 10%, it acts as an intermediate that suppresses the bioactivity and hence, leads to a decrease in the formation of HAp layer on the surfaces because of the lower reactivity of the crystalline state and increased resistance to the ion exchange reaction [42].

Another method to confirm the bioactivity by formation of an HAp layer on the surface of nanobioactive glass samples is XRF analysis. XRF results for the nanobioactive glass surfaces before and after SBF immersions are tabulated (Table 4). The above results confirm that the surface content of Ca^{2+} and P^{5+} increases, whereas the content of Si^{4+} decreases after immersion in SBF for a period of 21 day. After 21 day, the Ca/P ratio (1.63) is closer to an appropriate stoichiometric value (1.67) of HAp. The above result confirms the presence of HAp layer on the surface of 10% MgO-substituted nanobioactive glass samples (MT10). The surface area measurement is evident for the efficient formation of HAp layer due to the increased surface area of MT10 when compared with other compositions (MT0 and MT20).

The above results reveal that MT10 achieves better HAp layer deposition when compared with other MgO compositions. The observed *in vitro* bioactivity is higher, and better biocompatibility could be attained at MT10 which indicates good morphology for the glass structure. This result suggests that MT10 may be the optimum

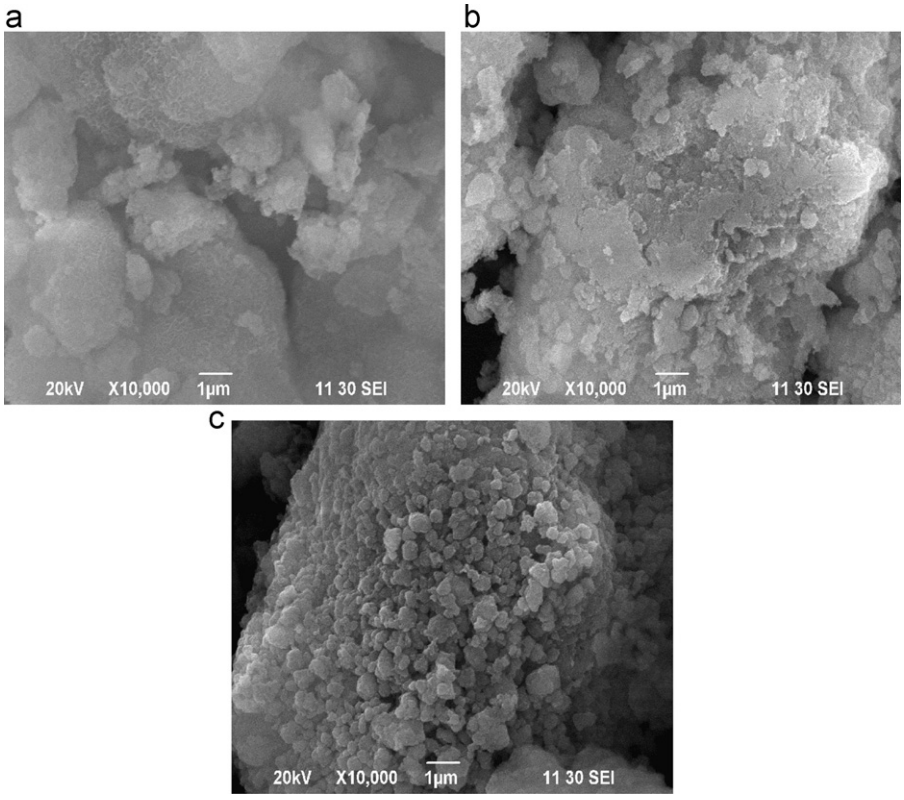

Fig. 9. SEM images of different nano bioactive glass samples after incubation in SBF for 21 day. (a) MT0, (b) MT10 and (c) MT20.

Table 4
Elemental analysis of bioactive glass surfaces before and after immersion in SBF by XRF.

Sample	Before immersion			After immersion			
	Si (wt%)	Ca (wt%)	P (wt%)	Si (wt%)	Ca (wt%)	P (wt%)	Ca/P
MT0	45.22	43.6	11.02	29.64	41.38	14.07	2.93
MT10	41.98	36.87	12.31	30.47	38.35	23.44	1.63
MT20	45.66	24.99	15.36	44.33	25.60	19.184	1.33

concentration for silica glass systems to be used in bone implant and other biomedical applications.

From the antimicrobial study, it is clear that MgO-substituted glass at various concentrations, namely B (10 μg L^{-1}), C (100 μg L^{-1}) and D (1000 μg L^{-1}), does not show any zone of inhibition for both *S. aureus* and *E. coli*, indicating clearly that it does not have antimicrobial property, which is shown in Figs. 10 and 11, respectively. From this observation, it is evident that MgO-based glass is non-reactive against bacteria.

In vitro cell viability assay is performed for the prepared nanobioactive glass samples. Nanobioactive glass sample-treated cell lines at a concentration of 100 μg ml^{-1} are observed microscopically for the cell damage (Fig. 12). The results show that MT10 are not showing any cell damage when compared with MT0 and MT20. Generally, nanobioactive glasses have a tendency to form the agglomeration in biological solution [43] and hence, it leads to solubility difficulties during *in vitro* study. But the nano particles improve the degradability in biological environment than the bulk and lead to better cell attachment and bone growth [44,45]. Cells are exposed to nanobioactive glass at a concentration of 100 μg ml^{-1} and their viability percentages are evaluated by MTT assay (Fig. 13). The result of all the nanobioactive glass samples at a concentration of 100 μg ml^{-1} indicates that they are non-toxic. A significant increase in cell viability is found in MT10 sample and a decrease in MT20 samples when compared with base glass (MT0). Magnesium ion shows evidence for the formation of apatite layer as well as cell attachment and proliferation due to its solubility and release of ions in body [20,46]. MT10 is the optimal concentration for the formation of HAp layer due to the release of ions that is essential for the cell attachment. In MT20 sample, cell viability and HAp layer formation are slow because of low dissolubility of glass sample and it leads to unfavourable environment for cell attachment and proliferation [47]. Therefore, magnesium-containing bioactive glass samples show higher biocompatibility than control in AGS cell lines and could essentially serve as an effective material for *in vivo* applications. As the concentration of magnesium increases above 10% in the bioactive glass sample, the cell viability decreases and some toxic effects are induced to cells. Cytotoxicity studies are also correlated with above results that 10% magnesium-substituted nanobioactive glass shows better bioactivity and biocompatibility.

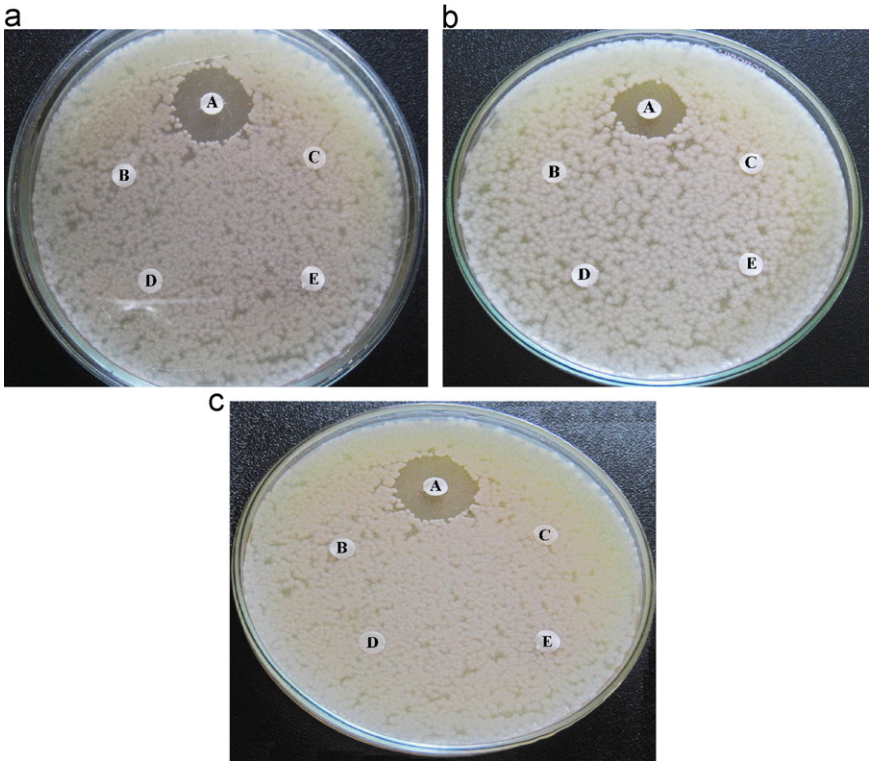

Fig. 10. Antimicrobial susceptibility test of nanobioactive glasses against *S. aureus* (A) positive control (Antibiotics) (B) 10 μg L^{-1} (C) 100 μg L^{-1} (D) 1000 μg L^{-1} and (E) Blank disc. (a) MT0, (b) MT10 and (c) MT20.

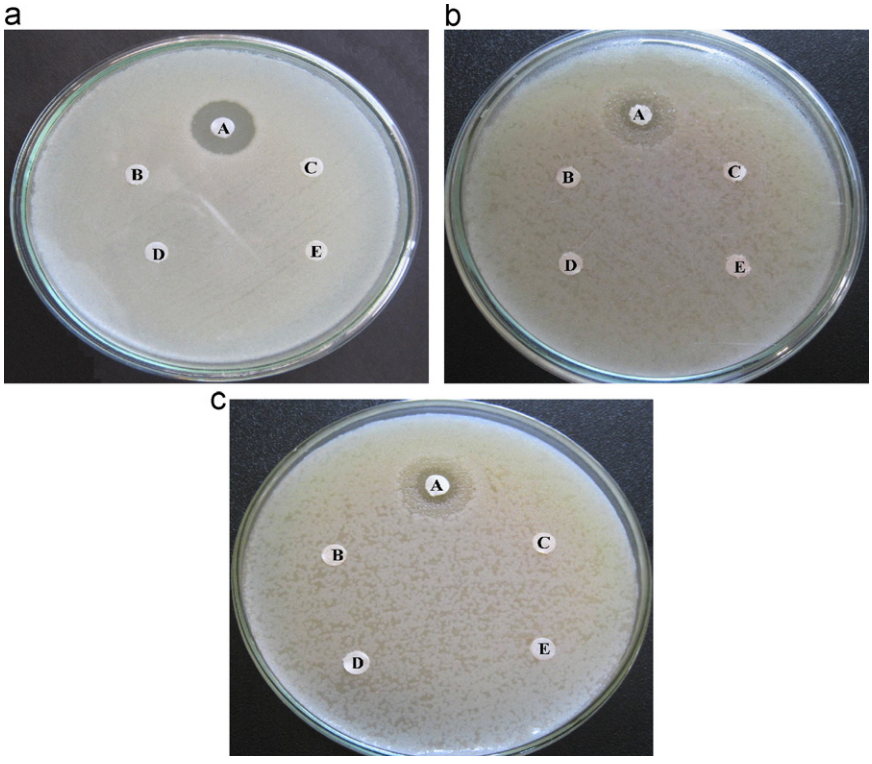

Fig. 11. Antimicrobial susceptibility test of nanobioactive glasses against *E. coli* (A) positive control (Antibiotics) (B) 10 μg L^{-1} (C) 100 μg L^{-1} (D) 1000 μg L^{-1} and (E) Blank disc. (a) MT0, (b) MT10 and (c) MT20.

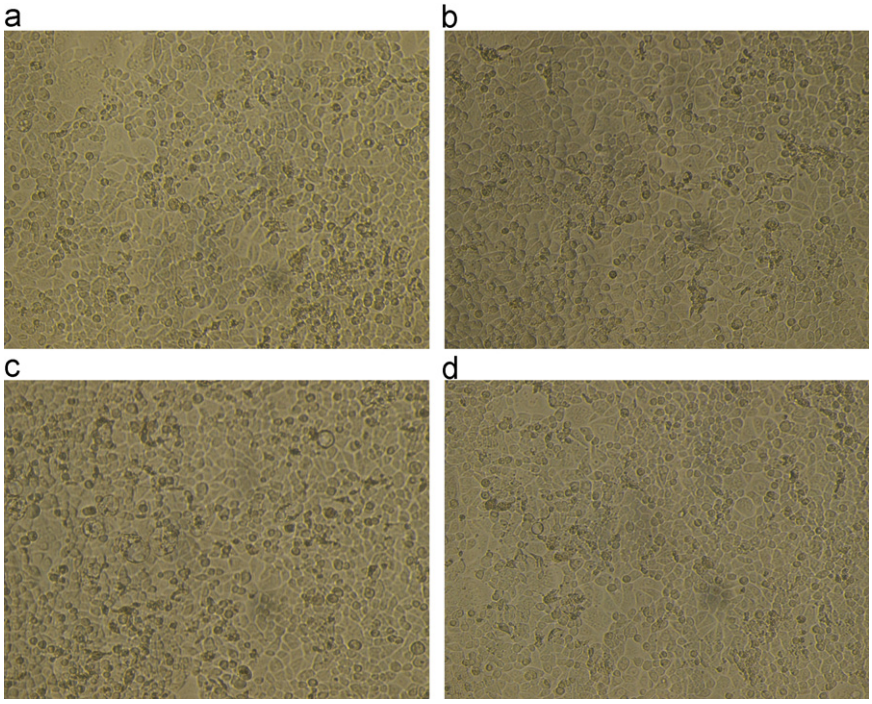

Fig. 12. Viability of AGS cell line treated with nanobioactive glasses (100 μg ml^{-1}) after cell culturing for 48 h. (a) Untreated, (b) MT0, (c) MT10 and (d) MT20.

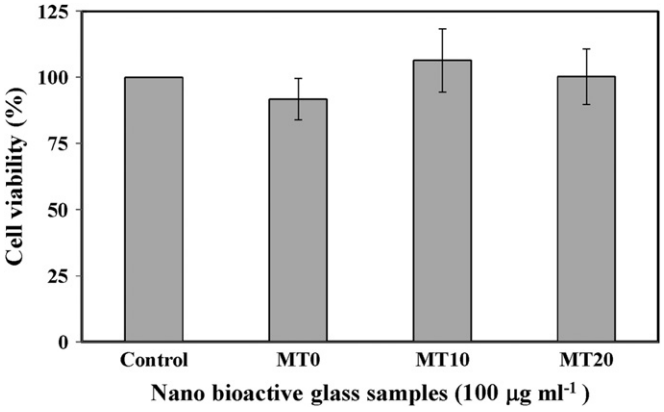

Fig. 13. *In vitro* cytotoxicity of prepared nanobioactive glasses by MTT assay in AGS cell line.

4. Conclusions

Nanobioactive glass samples substituted with different concentrations of magnesium (0, 10 and 20 mol%) are prepared using a sol–gel method. The bioactivity of the synthesized MgO glass samples is evaluated and compared with that of base glass. The presence of Mg in the glass composition increases the formation of the apatite layer when compared with base glass whereas the formation of HAp layer decreases when the concentration of Mg increases above 10%. The microbial study reveals that the prepared Mg-substituted glasses do not show any antibacterial activity. The cytotoxicity results show that the prepared glasses are non-toxic and exhibit better cell viability in MT10 at a concentration of 100 μg ml^{-1}. It is concluded that minimum 23% of calcium is essential in Mg-substituted bioactive glass to maintain the good bioactivity. The observed results indicate that the developed Mg-substituted bioactive glass samples could be the possible candidates for regenerative dentistry and implant applications with biocompatibility.

Acknowledgements

The authors are thankful to Department of Science and Technology (DST), New Delhi for the financial support to carry out this research project (SR/S2/CMP-0054/2009 dt. 27.09.2010). We would like to thank Dr. G. Kumaresan and Mr. P. Jayaprakash Department of Genetics, School of Biological Sciences, Madurai Kamaraj University (MKU), Madurai, for their assistance in the cell line studies with the support of Department of Atomic Energy (DAE)–MKU research project on ''Cancer Drug Discovery Assay Development''.

References

[1] L.L. Hench, Bioceramics: from concept to clinic, Journal of the American Ceramic Society 81 (1998) 1705–1728.
[2] C. Soundrapandian, S. Bharati, D. Basu, S Datta, Studies on novel bioactive glasses and bioactive glass-nano-HAp composites suitable for coating on metallic implants, Ceramics International 37 (2011) 759–769.
[3] L.C. Gerhardt, A.R. Boccaccini, Bioactive glass and glass-ceramic scaffolds for bone tissue engineering, Materials 3 (2010) 3867–3910.
[4] M. Peter, N.S. Binulal, S.V. Nair, N. Selvamurugan, H. Tamura, R. Jayakumar, Novel biodegradable chitosan-gelatin/nano-bioactive

glass ceramic composite scaffolds for alveolar bone tissue engineering, Chemical Engineering Journal 158 (2010) 353–361.
[5] P.M. Bartold, Y. Xiao, S.P. Lyngstaadas, M.L. Paine, M.L. Snead, Principles and applications of cell delivery systems for periodontal regeneration, Periodontology 41 (2006) 123–135.
[6] J. Zhong, D.C. Greenspan, Processing and properties of sol gel bioactive glasses, Journal of Biomedial Materials Research 53 (2000) 694–701.
[7] D. Zhao, N. Moritz, E. Vedel, L. Hupa, H.T. Aro, Mechanical verification of soft-tissue attachment on bioactive glasses and titanium implants, Acta Biomaterialia 4 (2008) 1118–1122.
[8] B. Saravanakumar, M. Rajkumar, V. Rajendran, Synthesis and characterisation of nanobioactive glass for biomedical applications, Materials Letters 65 (2011) 31–34.
[9] M.M. Pereira, A.E. Clark, L.L. Hench, Effect of texture on the rate of hydroxyapatite formation on gel silica surface, Journal of the American Ceramic Society 78 (1995) 2463–2468.
[10] R.M. Vallet-Regi, C.V. Ragel, A.J. Salinas, Glasses with medical applications, European Journal of Inorganic Chemistry 6 (2003) 1029–1042.
[11] W. Xia, J. Chang, Preparation and characterization of nano-bioactive-glasses (NBG) by a quick alkali-mediated sol–gel method, Materials Letters 61 (2007) 3251–3253.
[12] P. Saravanapavan, L.L. Hench, Low-temperature synthesis, structure and bioactivity of gel derived glasses in the binary $CaO–SiO_2$ system, Journal of Biomedial Materials Research 54 (2001) 608–618.
[13] P. Sepulveda, J.R. Jones, L.L. Hench, Bioactive sol–gel foams for tissue repair, Journal of Biomedial Materials Research 59 (2002) 340–348.
[14] P. Saravanapavan, J.R. Jones, R.S. Pryce, L.L. Hench, Bioactivity of gel–glass powders in the CaO-SiO2 system: a comparison with ternary (CaO–P2O5–SiO2) and quaternary glasses ($SiO_2–CaO–P_2O_5–Na_2O$), Journal of Biomedial Materials Research Part A 66 (2003) 110–119.
[15] R.L. Siqueira, O. Peitl, E.D. Zanotto, Gel-derived $SiO_2–CaO–Na_2O–P_2O_5$ bioactive powders: synthesis and in vitro bioactivity, Materials Science and Engineering C 31 (2011) 983–991.
[16] R. Li, A.E. Clark, L.L. Hench, An investigation of bioactive glass powders by sol–gel processing, Journal of Applied Biomaterials 2 (1991) 231–239.
[17] I. Gutowska, Z. Machoy, B. Machaliski, The role of bivalent metals in hydroxyapatite structures as revealed by molecular modeling with the HyperChem software, Journal of Biomedial Materials Research Part A.75A (2005) 788–793.
[18] E. Bertoni, A. Bigi, G. Cojazzi, M. Gandolfi, S. Panzavolta, N. Roveri, Nanocrystals of magnesium and fluoride substituted hydroxyapatite, Journal of Inorganic Biochemistry 72 (1998) 29–35.
[19] S. Ni, L. Chou, J. Chang, Preparation and characterization of forsterite (Mg_2SiO_4) bioceramics, Ceramics International 33 (2007) 83–88.
[20] A. Balamurugan, G. Balossier, J. Michel, S. Kannan, H. Benhayoune, A.H.S Rebelo, J.M.F. Ferreira, Sol gel derived $SiO_2–CaO–MgO–P_2O_5$ bio glass system-preparation and *in vitro* characterization, Journal of Biomedial Materials Research Part B 83 (2007) 546–553.
[21] J. Ma, C.Z. Chen, D.G. Wang, X. Shao, C.Z. Wang, H.M. Zhang, Effect of MgO addition on the crystallization and *in vitro* bioactivity of glass ceramics in the $CaO–MgO–SiO_2–P_2O_5$ system, Ceramics International, http://dx.doi.org/10.1016/j.ceramint.2012.05.056, in press.
[22] Y. Ebisawa, T. Kokubo, K. Ohura, T. Yamamuro, Bioactivity of $CaO \cdot SiO_2$-based glasses: *in vitro* evaluation, Journal of Materials Science: Materials in Medicine 1 (1990) 239–244.
[23] T. Kasuga, K. Nakagawa, M. Yoshida, E. Miyade, Compositional dependence of formation of an apatite layer on glass-ceramics in simulated physiological solution, Journal of Materials Science 22 (1987) 3721–3724.
[24] J.S. Moya, A.P. Tomsia, A. Pazo, C. Santos, F. Guitian, *In vitro* formation of hydroxyapatite layer in a MgO-containing glass, Journal of Materials Science Materials in Medicine 5 (1994) 529–532.
[25] J.M. Oliveira, R.N. Correia, M.H. Fernandes, Effects of Si speciation on the *in vitro* bioactivity of glasses, Biomaterials 23 (2002) 371–379.
[26] S. Ni, J. Chang, L. Chou, *In vitro* studies of novel $CaO–SiO_2–MgO$ system composite Bioceramics, Journal of Materials Science Materials in Medicine 19 (2008) 359–367.
[27] R.C. Bielby, I.S. Christodoulou, R.S. Pryce, W.J.P. Radford, L.L. Hench, J.M. Polak, Time and concentration-dependent effects of dissolution products of 58S sol–gel bioactive glass on proliferation and differentiation of murine and human osteoblasts, Tissue Engineering 10 (2004) 1018–1026.
[28] S. Brunauer, P.H. Emmett, E. Teller, Adsorption of gases in multimolecular layers, Journal of the American Chemical Society 60 (1938) 309–319.
[29] T. Kokubo, H. Takadama, How useful is SBF in predicting *in vivo* bone bioactivity? Biomaterials 27 (2006) 2907–2915.
[30] A. Bauer, W.M.M. Kirby, J.C. Sherris, M. Turch, Antibiotic susceptibility testing by a standardized single disk method, American Journal of Clinical Pathology 45 (1966) 493–496.
[31] E. Dietrich, H. Oudadesse, A. Lucas-Girot, M. Mami, *In vitro* bioactivity of melt-derived glass 46S6 doped with magnesium, Journal of Biomedial Materials Research 88A (2008) 1087–1096.
[32] D.C. Greenspan, J.P. Zhong, D.L. Wheeler, Bioactivity and biodegradability: melt *vs* sol–gel derived bioglass *in vitro* and *in vivo*, in: R.Z. LeGeros, J.P. LeGeros (Eds.), Bioceramics, 11, , 1998, p. 345.
[33] S. Kannan, F. Goetz-Neunhoeffer, J. Neubauer, S. Pina, P.M.C. Torres, J.M.F. Ferreira, Synthesis and structural characterization of strontium and magnesium-co-substituted β-tricalcium phosphate, Acta Biomaterialia 6 (2010) 571–576.
[34] E. Landi, S. Sprio, M. Sandri, G. Celotti, A. Tampieri, Development of Sr and CO_3 co-substituted hydroxyapatites for biomedical applications, Acta Biomaterialia 4 (2008) 656–663.
[35] A. Bigi, E. Boanini, C. Capuccini, M. Gazzano, Strontium-substituted hydroxyapatite nanocrystals, Inorganica Chimica Acta 360 (2007) 1009–1016.
[36] S.J. Watts, R.G. Hill, M.D. O'Donnell, R.V. Law, Influence of magnesia on the structure and properties of bioactive glasses, Journal of Non-Crystalline Solids 356 (2010) 517–524.
[37] P. Ducheyne, S. Radin, L. King, The effect of calcium phosphate ceramic composition and structure on *in vitro* behavior I. Dissolution, ‚Journal of Biomedical Materials Research 27 (1993) 25–34.
[38] K.S.K. Lin, T. Yao-Hung, Y. Mou, H. Yu-Chuan, Y. China-Min, J.C.C. Chan, Mechanistic study of apatite formation on bioactive glass surface using ^{31}P solid-state NMR spectroscopy, Chemical Material 17 (2005) 4493–4501.
[39] C. Ohtsuki, T. Kokubo, T. Yamamuro, Mechanism of apatite formation on CaO single bond SiO_2 single bond P_2O_5 glasses in a simulated body fluid, Journal of Non-Crystalline Solids 143 (1992) 84–92.
[40] P. Li, C. Ohtsuki, T. Kokubo, K. Nakanishi, N. Soga, T. Nakamura, T. Yamamuro, Process of formation of bone-like apatite layer on silica gel, Journal of Materials Science Materials in Medicine 4 (1993) 127–131.
[41] A. Martinez, I. Izquierdo-Barba, M. Vallet-Regi, Bioactivity of a $CaO–SiO_2$ binary glasses system, Chemical Materials 12 (2000) 3080–3088.
[42] K.E. Wallace, R.G. Hill, J.T. Pembroke, C.J. Brown, P.V. Hatton, Influence of sodium oxide content on bioactive glass properties, Journal of Materials Science Materials in Medicine 10 (1999) 697–701.
[43] A. Doostmohammadi, A. Monshi, M.H. Fathi, U. Pieles, A.U. Daniels, Preparation and physico-chemical characterization of bioactive glass nano particles agglomeration, European Cells and Materials 20 (2010) 61.
[44] S.K. Misra, T. Ansari, D. Mohn, S.P. Valappil, T.J. Brunner, W.J. Stark, I. Roy, J.C. Knowles, P.D. Sibbons, E.V. Jones, A.R. Boccaccini, V. Salih, Effect of nanoparticulate bioactive glass particles on bioactivity and cytocompatibility of poly(3-hydroxybutyrate) composites, Journal of the Royal Society, Interface 7 (2010) 453–465.
[45] S.K. Misra, D. Mohn, T.J. Brunner, W.J. Stark, S.E. Philip, I. Roy, V. Salih, J.C. Knowles, A.R. Boccaccini, Comparison of nanoscale

and microscale bioactive glass on the properties of P(3HB)/bioglass composites, Biomaterials 29 (2008) 1750–1761.
[46] J. Lu, J. Wei, Y. Yan, H Li, J. Jia, S. Wei, H. Guo, T. Xiao, C. Liu, Preparation and preliminary cytocompatibility of magnesium doped apatite cement with degradability for bone regeneration, Journal of Materials Science Materials in Medicine 22 (2011) 607–615.
[47] S. Ni, J. Chang, L. Chou, *In vitro* studies of novel CaO–SiO2–MgO system composite bioceramics, Journal of Materials Science Materials in Medicine 19 (2008) 359–367.
[48] H.S. Costa, M.F. Rocha, G.I. Andrade, E.F. Barbosa-Stancioli, M.M. Pereira, R.L. Orefice, W.L. Vasconcelos, H.S. Mansur, Sol–gel derived composite from bioactive glass–polyvinyl alcohol, Journal of Materials Science 43 (2008) 494–502.
[49] X. Yan, X. Huang, C. Yu, H. Deng, Y. Wang, Z. Zhang, S. Qiao, G. Lu, D. Zhao, The *in vitro* bioactivity of mesoporous bioactive glasses, Biomaterials 27 (2006) 3396–3403.
[50] Y. Zhang, M. Wang, A new methods to probe the structural evolution during the heat treatment of SiO_2–P_2O_5 gel glasses, Journal of Materials Science B 67 (1999) 99–101.
[51] B.D. Boyan, G. Niederaur, K. Kieswetter, N.C. Leatherbury, Biodegradable implant material comprising bioactive ceramic, United States patent 5977204 (1999).